CHEMISTRY
A EUROPEAN JOURNAL

ChemPubSoc
Europe

DOI: 10.1002/chem.201200940

VIP

Full Exploration of the Diels–Alder Cycloaddition on Metallofullerenes $M_3N@C_{80}$ (M = Sc, Lu, Gd): The D_{5h} versus I_h Isomer and the Influence of the Metal Cluster

Sílvia Osuna,[b] Ramón Valencia,[a] Antonio Rodríguez-Fortea,*[a] Marcel Swart,*[c, d] Miquel Solà,*[c] and Josep M. Poblet*[a]

Abstract: In this work a detailed investigation of the exohedral reactivity of the most important and abundant endohedral metallofullerene (EMF) is provided, that is, $Sc_3N@I_h$-C_{80} and its D_{5h} counterpart $Sc_3N@D_{5h}$-C_{80}, and the (bio)chemically relevant lutetium- and gadolinium-based $M_3N@I_h/D_{5h}$-C_{80} EMFs (M = Sc, Lu, Gd). In particular, we analyze the thermodynamics and kinetics of the Diels–Alder cycloaddition of s-*cis*-1,3-butadiene on all the different bonds of the I_h-C_{80} and D_{5h}-C_{80} cages and their endohedral derivatives. First, we discuss the thermodynamic and kinetic aspects of the cycloaddition reaction on the hollow fullerenes and the two isomers of $Sc_3N@C_{80}$. Afterwards, the effect of the nature of the metal nitride is analyzed in detail. In general, our BP86/TZP//BP86/DZP calculations indicate that [5,6] bonds are more reactive than [6,6] bonds for the two isomers. The [5,6] bond D_{5h}-**b**, which is the most similar to the unique [5,6] bond type in the icosahedral cage, I_h-**a**, is the most reactive bond in $M_3N@D_{5h}$-C_{80} regardless of M. $Sc_3N@C_{80}$ and $Lu_3N@C_{80}$ give similar results; the regioselectivity is, however, significantly reduced for the larger and more electropositive M = Gd, as previously found in similar metallofullerenes. Calculations also show that the D_{5h} isomer is more reactive from the kinetic point of view than the I_h one in all cases which is in good agreement with experiments.

Keywords: cycloaddition · density functional calculations · Diels–Alder reaction · fullerenes · thermodynamics

Introduction

Endohedral metallofullerenes (EMFs), that is, those fullerenes that contain metal atoms or metal clusters in their interior, have attracted increasing attention over the last few years due to their potential applications in different fields such as medicine or materials science.[1] Since the first detection of $La@C_{60}$ twenty-five years ago,[2] many different families of EMFs have been characterized. In 1999, Dorn and co-workers reported the synthesis, isolation, and characterization of $Sc_3N@I_h$-C_{80},[3] which is the third most abundant fullerene after C_{60} and C_{70} and the prototype of the family of nitride EMFs. Many other fullerenes that contain the trimetallic nitride unit have been prepared and characterized so far with carbon cages that range from C_{68} to C_{104} and with metal atoms that are generally from Group 3 or lanthanides.[1b,c] The electronic structure of the nitride EMFs can be easily understood from the ionic model if we consider that a formal transfer of six electrons from the internal guest to the carbon cage takes place, $(M_3N)^{6+}@(C_{2n})^{6-}$. Within this simple model, an orbital rule for predicting the most appropriate carbon-cage isomers to encapsulate a metal nitride was proposed by Poblet and co-workers.[4] The authors showed that the large HOMO–LUMO gap observed in nitride EMFs, which confers stability upon them, can be estimated from the energy gap between the LUMO+3 and the LUMO+2 in the empty cages. Popov and Dunsch showed that, in general, the stabilities of C_{2n}^{6-} and $M_3N@C_{2n}$ match, thereby confirming the validity of the ionic model.[5] The molecular orbital rule, although very useful, does not provide the physical explanation for the selection of a particular host C_{2n} cage by a given metal cluster. Recently, it has been shown that the relative stabilities of

[a] Dr. R. Valencia, Dr. A. Rodríguez-Fortea, Prof. J. M. Poblet
Departament de Química Física i Inorgànica
Universitat Rovira i Virgili, c/Marcel·lí Domingo s/n
Campus Sescelades, 43007 Tarragona (Spain)
E-mail: antonio.rodriguezf@urv.cat
josepmaria.poblet@urv.cat

[b] Dr. S. Osuna
Department of Chemistry and Biochemistry
University of California, Los Angeles
607 Charles E. Young Drive
Los Angeles, CA 90095 (USA)

[c] Prof. M. Swart, Prof. M. Solà
Institut de Química Computacional i
Departament de Química
Universitat de Girona, Campus Montilivi s/n
17071 Girona (Spain)
E-mail: marcel.swart@udg.edu
miquel.sola@udg.edu

[d] Prof. M. Swart
Institució Catalana de Recerca i Estudis Avançats (ICREA)
Pg. Lluís Companys 23, 08010 Barcelona (Spain)

Supporting information for this article is available on the WWW under http://dx.doi.org/10.1002/chem.201200940.

hollow C_{2n}^{6-} isomers depend on the separation among pentagons, which localize more negative charge than hexagons.[6]

The charge transfer from the encapsulated cluster to the fullerene cage provides unique properties to EMFs that confer onto them a characteristic reactivity relative to their hollow counterparts. Exohedral functionalization of EMFs is crucial to obtain new materials for multiple potential applications. For instance, water-soluble derivatives of $Gd_3N@I_h$-C_{80} have been shown to be effective relaxation agents for magnetic resonance imaging (MRI).[7] The first functionalization of a nitride EMF to be described was the Diels–Alder cycloaddition on the icosahedral (I_h) isomer $Sc_3N@C_{80}$, reported by Iezzi et al. in 2002.[8] Due to the high symmetry of the I_h-C_{80} cage, only two different regioisomers are possible after functionalization: the adduct on a [5,6] ring junction (Figure 1, type D) or the adduct on a [6,6] ring

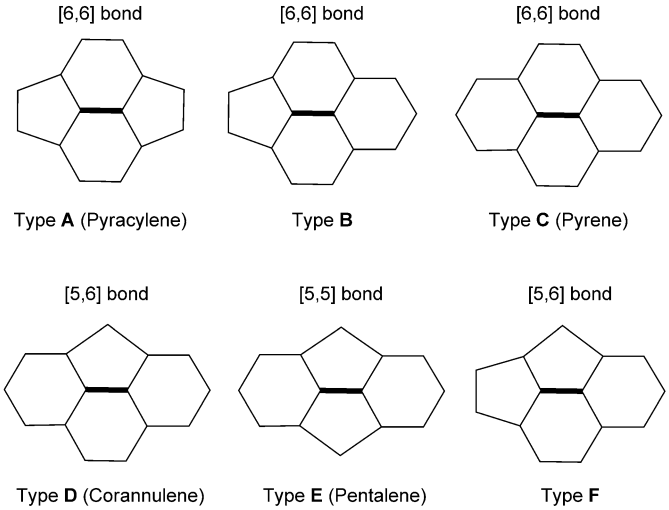

Figure 1. Different C–C bond types that may be present in a fullerene.

junction (Figure 1, type B). DFT calculations at BP86/TZP level have shown that addition in the corannulene [5,6] bond (type D) is at least 11 kcal mol^{-1} more stable than the adduct on the [6,6] bond.[9] 1,3-Dipolar cycloadditions of azomethine ylides (the so-called Prato reaction) on $M_3N@I_h$-C_{80} show a variety of interesting results. For the *N*-ethylazomethine ylide, the addition takes place regioselectively at the corannulene [5,6] bond on $Sc_3N@I_h$-C_{80}, but the two regioisomers can be observed when the cycloaddition occurs on $Y_3N@I_h$-C_{80}.[10] The two adducts are also observed in the synthesis of *N*-tritylpyrrolidino derivative of $Sc_3N@I_h$-C_{80}.[11] In the case of the Bingel–Hirsch cyclopropanation of diethylbromomalonate on $M_3N@I_h$-C_{80}, addition takes place on the [6,6] bond for M = Sc, Lu, Y, and Er, but the Y- and Er-based EMFs are much more reactive than the others.[12] Therefore, as pointed out previously, the exohedral reactivity of the EMFs seems to be dictated by the nature of the encapsulated metal cluster. In a theoretical study, Rodriguez-Fortea et al. reported that the [5,6] pyrrolidino adduct of $Sc_3N@I_h$-C_{80} is much more stable than the [6,6] regioisomer; however, the two regioisomers are almost degenerate for $Y_3N@I_h$-C_{80}.[13] Furthermore, the [6,6] adduct is found to be the kinetic product as in experiments. A pirouette-type mechanism was proposed for the observed [6,6]-to-[5,6] isomerization under thermal conditions instead of by means of retrocycloaddition.[13]

Other cages with lower symmetries that encapsulate metal clusters show a larger number of different C–C bonds, thus increasing the possible quantity of regioisomers (Figure 1). Dorn and co-workers have synthesized and functionalized the cage isomers $M_3N@D_{5h}$-C_{80} (M = Sc and Lu) by means of Diels–Alder and Prato cycloadditions.[14] Interestingly, the D_{5h}-C_{80} isomer was found to be significantly more reactive than the I_h-C_{80} one, regardless of the metal nitride, as previously observed by Stevenson et al. for the reaction with diamino silica.[15] Cai et al. synthesized the *N*-tritylpyrrolidino derivatives of $Sc_3N@D_{3h}$-C_{78} and, by means of NMR spectroscopic experiments and X-ray crystallography, found that addition took place over two different type-B [6,6] bonds and not over the type-A [6,6] pyracylene bond,[16] the most reactive bond in C_{60}. The same group observed that Bingel–Hirsch cyclopropanation of bromomethylmalonate on $Sc_3N@D_{3h}$-C_{78} and $Sc_3N@D_3$-C_{68} also occurs on type-B [6,6] bonds.[17] Recently, some of us performed a theoretical study of the thermodynamics and kinetics of the Diels–Alder reaction of s-*cis*-1,3-butadiene and $Sc_3N@D_{3h}$-C_{78}.[18] The results showed that encapsulation of the nitride on the carbon cage produces a decrease in its reactivity, and those bonds with Sc atoms facing them become un- or less reactive. Moreover, the reactions over the hollow fullerene and the EMF lead to totally different cycloadducts. The thermodynamic product on the EMF, which is also predicted to be the kinetic product, is found on a type-B [6,6] bond and matches the lowest-energy *N*-tritylpyrrolidino adduct on $Sc_3N@D_{3h}$-C_{78}.[16] The stability of products and the reaction barriers for the Diels–Alder cycloaddition on two cage isomers of $Y_3N@C_{78}$, the isolated pentagon rule (IPR) $D_{3h}(5)$ and the non-IPR $C_2(22010)$, were also analyzed.[19] Release of the strain energy of the cages plays the most important role in the reactivity of these isomers. Likewise, addition to the type-E pentalene bond is predicted on the non-IPR $C_2(22010)$ cage. Moreover, the regioselectivity of the Diels–Alder reaction of s-*cis*-1,3-butadiene to $Ti_2C_2@C_{78}$ EMF has been recently studied and has been found to be quite different from that of the $Sc_3N@D_{3h}$-C_{78} EMF due to the orientation of the metallic cluster.[20] Finally, a DFT study of the Bingel–Hirsch cyclopropanation on non-IPR $Gd_3N@C_{2n}$ ($2n = 82$ and 84) confirmed that the release of strain in the fullerene due to functionalization and formation of open-cage fullerenoids is crucial to understanding the reactivity of such non-IPR EMFs.[21]

The computational exploration of the exohedral reactivity of EMFs has been shown to be a powerful tool to understand, predict, and support the experimental addition sites.[22] The aim of the present work is to provide a detailed investigation of the exohedral reactivity of the most impor-

tant and abundant EMFs, that is, the $Sc_3N@I_h$-C_{80} and its $Sc_3N@D_{5h}$-C_{80} isomer, and the (bio)chemically relevant lutetium- and gadolinium-based EMFs for both I_h and D_{5h} cages. In particular, we analyze the thermodynamics and the kinetics of the Diels–Alder cycloaddition of s-*cis*-1,3-butadiene on all the different bonds of the I_h-C_{80} and D_{5h}-C_{80} cages. First, we discuss the thermodynamic and kinetic aspects of the cycloaddition on the hollow fullerenes and the two isomers of $Sc_3N@C_{80}$. Afterwards, the effect of the nature of the metal nitride is analyzed in detail.

Computational Methods

All density functional theory calculations have been performed with the Amsterdam Density Functional (ADF) program.[23] The molecular orbitals (MOs) were expanded in an uncontracted set of Slater-type orbitals (STOs) of double-ζ (DZP) and triple-ζ (TZP) quality that contained diffuse functions and one set of polarization functions. Core electrons (1s for second period, 1s2s2p for third to fourth period, 1s2s2p3s3p4s3d4p5s4d for sixth period) were not treated explicitly during the geometry optimizations (frozen core approximation),[23b] as it was shown to have a negligible effect on the obtained geometries.[24] An auxiliary set of s, p, d, f, and g STOs was used to fit the molecular density and to represent the Coulomb and exchange potentials accurately for each self-consistent field (SCF) cycle. Energies and gradients were calculated using the local density approximation (Slater exchange and VWN correlation)[25] with nonlocal corrections for exchange (Becke88)[26] and correlation (Perdew86)[27] included self-consistently (i.e., the BP86 functional). Scalar relativistic corrections have been included self-consistently by using the zeroth-order regular approximation (ZORA).[28]

All energies reported here have been obtained with the TZP basis in single-point energy calculations at geometries that were obtained with the DZP basis (i.e., BP86/TZP//BP86/DZP). Although it is well documented that standard DFT functionals like BP86 underestimate energy barriers[29] (in the case of the parent Diels–Alder reaction BP86/TZP predicts a barrier of 18.6 kcal mol^{-1}, that is, an underestimation of the experimental value by some 6 kcal mol^{-1}), this underestimation should be similar for all Diels–Alder transition states we encounter here.

The actual geometry optimizations and TS searches were performed with the QUILD[30] (QUantum-regions Interconnected by Local Descriptions) program, which functions as a wrapper around the ADF program. The QUILD program constructs all input files for ADF, runs ADF, and collects all data; ADF is used only for the generation of the energy and gradients. Furthermore, the QUILD program uses improved geometry optimization techniques, such as adapted delocalized coordinates[31] and specially constructed model Hessians with the appropriate number of eigenvalues.[30] The latter is of particular use for TS searches. All TSs that correspond to the Diels–Alder addition to the free cages, and scandium- and lutetium-based EMFs have been characterized by computing the analytical[32] vibrational frequencies, to have one imaginary frequency corresponding to the approach of the two reacting carbon atoms. We should mention here that the optimization of the gadolinium-based compounds has been a difficult task. Gadolinium atoms have an incomplete f shell ($[Xe]4f^75d^16s^2$), and therefore different spin configurations for $Gd_3N@C_{80}$ are possible. The seven unpaired electrons of the gadolinium atoms can be coupled either ferromagnetically ($S=^{21}/_2$) or antiferromagnetically ($S=^7/_2$). The difference in energy between the latter two configurations was found to be extremely low (0.1 kcal mol^{-1}).[33] It was also recently published that the low-spin state in the case of the related compound $Gd_3N@C_{78}$ is 4.5 meV (≈0.1 kcal mol^{-1}) lower in energy than the high-spin state.[34] All calculations reported here have been performed considering the antiferromagnetic coupling (i.e., $S=^7/_2$). In practice, the analytical vibrational frequencies for the TSs of the gadolinium-based EMFs were not calculated due to the high computational cost and SCF convergence difficulties related with the high number of unpaired electrons, and based on the similarities of the TS structures with those of the other metal clusters. Pyramidalization angles introduced by Haddon[35] were computed using the POAV3 program.[36]

Results and Discussion

The Diels–Alder reaction between s-*cis*-1,3-butadiene and the fullerenes I_h-C_{80}, D_{5h}-C_{80}, $M_3N@I_h$-C_{80}, and $M_3N@D_{5h}$-C_{80} (M = Sc, Lu, and Gd) has been thoroughly studied for all the nonequivalent bonds that exist in the two fullerene cages. For the highly symmetrical I_h-C_{80} cage, only two different addition sites are possible: a type-D [5,6] (corannulene) ring junction and a type-B [6,6] junction (Figures 1 and 2). For the less symmetric D_{5h}-C_{80} isomer, nine different C–C bonds exist (Figure 2); four of them are [5,6] bonds

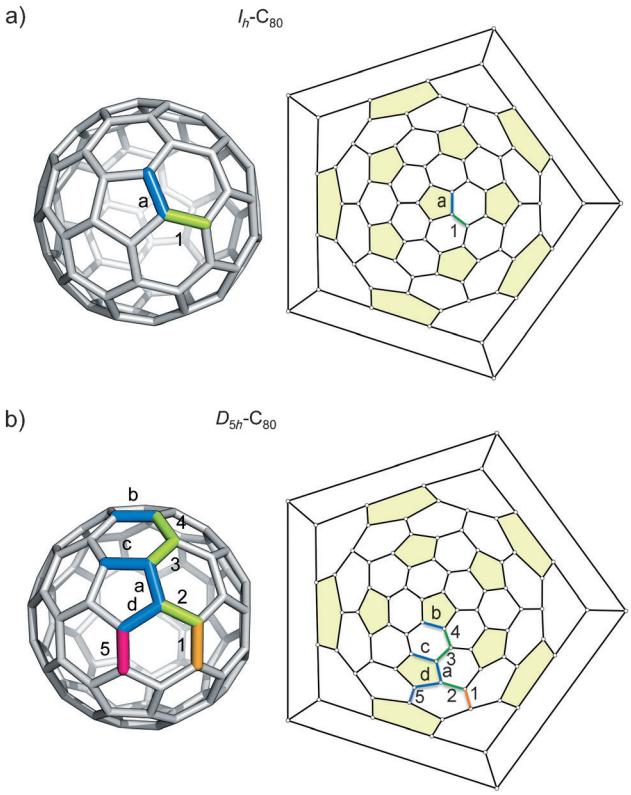

Figure 2. Different nonequivalent bonds of the a) I_h-C_{80} and b) D_{5h}-C_{80} cages are represented. Numbers denote [6,6] bonds and lower-case letters denote [5,6] bonds. Different colors are used to highlight the different bond types (pink is for type A, green for type B, orange for type C, and blue is for type D, according to Figure 1). The Schlegel diagrams, which convert the 3D fullerene into a 2D representation, for the two cage isomers are also shown.

(type-D) and five [6,6] bonds (one type-A, three type-B, and one type-C; see Figure 1). We will refer to each different bond according to the nomenclature used in Figure 2, in which numbers denote [6,6] bonds and lower-case letters denote [5,6] bonds. The study of the reactivity on the $M_3N@C_{80}$ EMFs is not straightforward because the metal ni-

tride can rotate in the interior of the carbon cage, as observed in NMR spectroscopic experiments[3,37] and computations.[13,38] We have considered eight orientations of the M_3N unit (see Figure 3) inside the I_h-C_{80} cage, but only five orientations (1, 2, 4, 5, and 8) have been chosen for the D_{5h}-C_{80} isomer. On the basis of our experience with other systems,

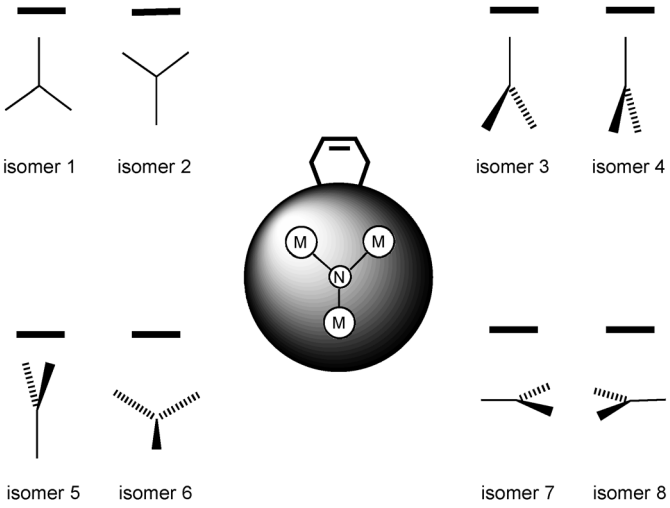

Figure 3. Representations of the relative position of the metal nitride (shown as a Y-shaped figure) with respect to the C–C bond of the fullerene where the adduct is formed (indicated by a bar) for the different isomers computed in this work.

we believe that these five orientations are sufficient to find the most favorable orientations for all nine nonequivalent bonds.[13,21] We refer to these as orientational isomers, which we identify with a subscript ranging from 1 to 8. For instance, $\mathbf{1_2}$ indicates that the addition has been produced over the [6,6] bond **1** (Figure 2) and that the metallic cluster is oriented as in orientational isomer 2 (Figure 3).

Reaction energies for Diels–Alder cycloaddition on $Sc_3N@I_h$-C_{80} and $Sc_3N@D_{5h}$-C_{80}

Isomer I_h: We have analyzed the thermodynamics of the [4+2] Diels–Alder reaction between s-*cis*-1,3-butadiene and empty I_h-C_{80} and $Sc_3N@I_h$-C_{80}. In the case of the hollow fullerene, the preferred addition site corresponds to the type-D [5,6] bond (the reaction energy is $-27.9\,kcal\,mol^{-1}$; see Table 1). In contrast, the cycloaddition reaction over the type-B [6,6] bond is approximately $16\,kcal\,mol^{-1}$ less exothermic (Table 1). As already observed by Campanera et al.,[9] C–C bond lengths and pyramidalization angles, θ_p, in the pristine fullerene cage may be used as predictors for the reactivity of the different bond types within the molecule. As pointed out in previous studies,[9,18] the Diels–Alder reaction should be favored for bonds with short lengths and high pyramidalization angles, although exceptions exist.[18,19] Bonds $\boldsymbol{I_h}$**-1** and $\boldsymbol{I_h}$**-a** both have similar lengths, but the pyramidalization angle for $\boldsymbol{I_h}$**-a** is much larger than for $\boldsymbol{I_h}$**-1** (Table 1). This must be the origin of their different reactivity. It is worth noting that this is the opposite situation found for the most common C_{60} and C_{70} fullerenes for which the [6,6] are much more reactive than the [5,6] bonds.[39] However, it should be emphasized that I_h-C_{80} lacks the highly reactive [6,6] pyracylene bond.

Once the Sc_3N cluster is encapsulated inside the cage, the cycloaddition reaction is also basically preferred over the [5,6] bond. The preferred orientational isomers $\boldsymbol{I_h}$**-a**$_6$ and $\boldsymbol{I_h}$**-a**$_2$ present reaction energies of -17.2 and $-15.6\,kcal\,mol^{-1}$, respectively (see Table 2 and Table S1 in the Supporting Information, and Figure 4). These cycloadducts have the scandium atoms of the metallic cluster situated far away from the bond at which the s-*cis*-1,3-butadiene has been attached. However, the nitride cluster and the attacked bond are either situated in the same plane ($\boldsymbol{I_h}$**-a**$_2$) or the Sc_3N unit is slightly tilted ($\boldsymbol{I_h}$**-a**$_6$) (see Figures 3 and 4). This trend of scandium-based nitride fullerenes for reacting with bonds

Table 1. C–C bond lengths and pyramidalization angles in the hollow I_h-C_{80} and D_{5h}-C_{80} reactants along with the reaction energies, reaction barriers, and C–C bond lengths in the transition states and final Diels–Alder adducts.[a–d]

		Reactants		DA adducts			Transition states		
Bond	Bond type[b]	R_{full}	θ_p	ΔE_R	R_{full}	Type	$\Delta E^{\neq}$		R_{CC}
I_h-C_{80}									
$\boldsymbol{I_h}$**-1**	B [6,6]	1.428	9.62	−11.6	1.435	asyn	2.9	1.609	2.536
$\boldsymbol{I_h}$**-a**	D [5,6]	1.438	10.58	−27.9	1.423	asyn	3.8	2.118	2.941
D_{5h}-C_{80}									
$\boldsymbol{D_{5h}}$**-1**	C [6,6]	1.471	8.64	0.5	1.660	asyn	20.2	1.922	3.002
$\boldsymbol{D_{5h}}$**-2**	B [6,6]	1.425	9.67	−16.1	1.612	asyn	10.2	2.048	3.027
$\boldsymbol{D_{5h}}$**-3**	B [6,6]	1.425	9.50	−3.5	1.605	asyn	10.9	2.049	3.083
$\boldsymbol{D_{5h}}$**-4**	B [6,6]	1.430	9.71	−4.8	1.596	asyn	7.1[d]	2.119	3.378
$\boldsymbol{D_{5h}}$**-5**	A [6,6]	1.382	10.66	−20.6	1.550	syn	10.8	2.373	2.272
$\boldsymbol{D_{5h}}$**-a**	D [5,6]	1.432	10.50	−24.7	1.612	syn	15.9	1.946	2.000
$\boldsymbol{D_{5h}}$**-b**	D [5,6]	1.435	10.73	−28.2	1.604	asyn	8.1	2.172	2.976
$\boldsymbol{D_{5h}}$**-c**	D [5,6]	1.451	10.31	−22.7	1.616	asyn	10.4	2.057	3.075
$\boldsymbol{D_{5h}}$**-d**	D [5,6]	1.444	10.68	−19.0	1.596	asyn	12.1	2.007	3.075

[a] Bond lengths, R_{full} and R_{CC} [Å], and average pyramidalization angles of the two C atoms involved in the bond, θ_p [°]; R_{full} is the length of the C–C bond over which the reaction took place, and R_{CC} are the bond lengths of the two newly formed C–C bonds. [b] Bond-type classification according to Figure 1. [c] Reaction energies, ΔE_R, and reaction barriers, $\Delta E^{\neq}$ [$kcal\,mol^{-1}$].[d] TS computed in the triplet state (all attempts to converge the singlet state were unsuccessful due to the tiny HOMO–LUMO gap).

Table 2. Reaction energies, reaction barriers, and bond lengths in the transition states and the final products of the Diels–Alder addition on the EMFs $Sc_3N@I_h$-C_{80} and $Sc_3N@D_{5h}$-C_{80}.[a–d]

		DA adducts			Transition states		
Bond	Bond type[b]	ΔE_R	R_{CC}		Type	$\Delta E^{\neq}$	R_{CC}
$Sc_3N@I_h$-C_{80}							
$\boldsymbol{I_h}$**-a$_6$**	D [5,6]	−17.2	1.559	1.558	asyn	15.7	1.891	2.871
$\boldsymbol{I_h}$**-1$_6$**	B [6,6]	−4.4	1.579	1.565	asyn	19.3[d]	2.614	1.784
$Sc_3N@D_{5h}$-C_{80}							
$\boldsymbol{D_{5h}}$**-b$_2$**	D [5,6]	−15.8	1.555	1.561	asyn	13.4	1.915	2.904
$\boldsymbol{D_{5h}}$**-c$_2$**	D [5,6]	−14.1	1.559	1.557	asyn	16.2	1.839	3.011
$\boldsymbol{D_{5h}}$**-3$_5$**	B [6,6]	−10.0	1.572	1.571	asyn	16.4	1.891	2.665
$\boldsymbol{D_{5h}}$**-a$_2$**	D [5,6]	−9.2	1.562	1.562	asyn	16.5	1.674	2.743
$\boldsymbol{D_{5h}}$**-d$_1$**	D [5,6]	−8.7	1.560	1.560	asyn	17.2	1.890	2.795
$\boldsymbol{D_{5h}}$**-2$_5$**	B [6,6]	−8.1	1.574	1.573	syn	17.4	2.275	2.554
$\boldsymbol{D_{5h}}$**-5$_8$**	A [6,6]	−2.0	1.575	1.576	asyn	18.4	1.775	3.261
$\boldsymbol{D_{5h}}$**-1$_5$**	C [6,6]	−1.6	1.575	1.575	asyn	21.7	1.876	2.405
$\boldsymbol{D_{5h}}$**-4$_1$**	B [6,6]	1.2	1.565	1.572	syn	21.9	2.083	2.234

[a] Reaction energies (ΔE_R) and barriers ($\Delta E^{\neq}$) [kcal mol^{-1}], and bond lengths [Å]. [b] Bond-type classification according to Figure 1. [c] Only the lowest-energy orientational isomer for each regioisomer is shown. The complete table with all the studied adducts can be found in the Supporting Information. [d] The lowest-energy barrier for the $\boldsymbol{I_h}$**-1** regioisomer corresponds to the orientational isomer 5 ($\boldsymbol{I_h}$**-1$_5$**).

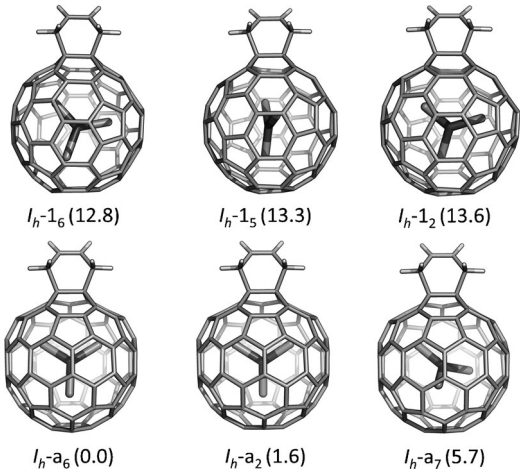

Figure 4. Representation of the regioisomers obtained from the Diels–Alder cycloaddition between s-*cis*-1,3-butadiene and $Sc_3N@I_h$-C_{80}. The lowest-energy orientations of the Sc_3N cluster for each regioisomer are shown; [6,6] and [5,6] regioisomers are named $\boldsymbol{I_h}$**-1$_x$** and $\boldsymbol{I_h}$**-a$_x$**, respectively, for which ***x*** denotes the orientation of the metal nitride, according to Figure 3. In parenthesis, the relative energies [kcal mol^{-1}] with respect to the lowest-energy $\boldsymbol{I_h}$**-a$_6$** isomer. All the computed adducts can be found in the Supporting Information.

situated far away from the Sc_3N influence is not unexpected. In the case of $Sc_3N@D_{3h}$-C_{78}, in which the nitride unit does not freely rotate, it was found that those bonds that present one of the scandium atoms faced towards them were highly deactivated versus s-*cis*-1,3-butadiene relative to empty C_{78}.[18] Similar results were found for 1,3-dipolar cycloadditions with azomethine ylides (Prato reaction).[13] Therefore, our theoretical exploration of the chemical reactivity of $Sc_3N@I_h$-C_{80} is in line with the experimental findings and previous computations.[9,18] The orientational isomer that presents the third most exothermic reaction energy corresponds to $\boldsymbol{I_h}$**-a$_7$** (−11.5 kcal mol^{-1}). In this case, the nitride unit is also situated far away from the attacked [5,6] bond, but the Sc_3N unit is not located in the same plane as the C–C bond. The rest of the isomers that correspond to the [5,6] addition present very low reaction energies that range from −4.0 to −6.8 kcal mol^{-1} (Table S1 in the Supporting Information). The Diels–Alder reaction over [6,6] bonds is highly unfavorable; the reaction energies range from 0.4 to −4.4 kcal mol^{-1}. Again, those orientations of the nitride cluster in which the scandium atoms are not in close contact with the reactive bond (i.e., $\boldsymbol{I_h}$**-1$_5$** and $\boldsymbol{I_h}$**-1$_6$**) present the most exothermic reaction energies (−3.9 and −4.4 kcal mol^{-1}, respectively). It is interesting to note that rotation of the cluster is more hindered when the bond is functionalized, as previously noted for other reactions.[12,13,40]

Isomer D_{5h}: For the reaction with the empty D_{5h}-C_{80} (Table 1), we observed that most of the reaction energies are exothermic and of the same magnitude as those found for the empty I_h-C_{80} and D_{3h}-C_{78}.[18] In general, [5,6] bonds are more reactive than [6,6] bonds; the reaction energies for the four [5,6] bonds are all exothermic in the range from −28.2 to −19.0 kcal mol^{-1}. Except for the pyracylene-type bond $\boldsymbol{D_{5h}}$**-5** and the type-B bond $\boldsymbol{D_{5h}}$**-2**, the reactivity of the [6,6] bonds is very low. The behavior for D_{5h}-C_{80} is similar to that found for the D_{3h}-C_{78} cage: the most reactive bond is a [5,6] bond of type D and the most reactive [6,6] bond is of pyracylene type (A). In the present case, the most exothermic reaction energy is obtained when the addition takes place on [5,6] bond $\boldsymbol{D_{5h}}$**-b** (−28.2 kcal mol^{-1}). This bond shows a rather short length (1.435 Å) and the largest pyramidalization angle (10.73°), see Table 1. The remaining three [5,6] bonds ($\boldsymbol{D_{5h}}$**-a**, $\boldsymbol{D_{5h}}$**-c**, and $\boldsymbol{D_{5h}}$**-d**) feature similar or slightly larger lengths and somewhat smaller pyramidalization angles. In contrast, [6,6] bonds show, except for the pyracylene-type bond $\boldsymbol{D_{5h}}$**-5**, smaller pyramidalization angles than [5,6] bonds in line with their lower reactivity. Bond $\boldsymbol{D_{5h}}$**-5**, with the shortest C–C length (1.382 Å) and a high pyramidalization angle (10.66°), yields the fourth most exothermic reaction energy after bonds $\boldsymbol{D_{5h}}$**-b**, $\boldsymbol{D_{5h}}$**-a**, and $\boldsymbol{D_{5h}}$**-c**. As in the case of the D_{3h}-C_{78} cage, the least reactive of all is bond $\boldsymbol{D_{5h}}$**-1** of pyrene-type (C), with the longest length

(1.471 Å) and the smallest pyramidalization angle (8.64°). Therefore, the C–C bond lengths and especially the pyramidalization angles predict correctly the general reactivity for most of the different bond types, but they do not allow distinguishing among bonds that show similar values of these two predictors, as, for example, bonds ***D*$_{5h}$-2** and ***D*$_{5h}$-4** with significantly different reactivity and similar values for the two predictors. Inspection of the topology of the LUMOs helps to understand such differences, as found previously for the D_{3h}-C_{78} cage.[18] The larger the contributions of the C atoms for a certain C–C bond in the LUMOs, the more reactive the bond will be. However, the lobes of the LUMOs within any of these bonds should be of the opposite sign so as to facilitate the [4+2]-cycloaddition reaction.

Bonds ***D*$_{5h}$-a**, ***D*$_{5h}$-b**, ***D*$_{5h}$-c**, and ***D*$_{5h}$-5** have suitable low-energy LUMOs with large contributions on the C atoms of the corresponding bonds to interact with the HOMO of the diene. Indeed, they are the bonds that yield the four most exothermic reactions. Therefore, the molecular orbitals of the fullerene reactants give predictions of the reactivity that agree qualitatively with the computed reaction energies. A combination of the three criteria allows, however, a better prediction of the relative reactivity of the different bonds.[18,22]

Regarding the Diels–Alder reaction on $Sc_3N@D_{5h}$-C_{80}, for each of the different bonds we have computed five different orientations of the metal nitride inside the fullerene (1, 2, 4, 5, and 8; see Figure 3) based on our experience with previous studies.[13,21] The reaction energies, displayed in Table 2 (Table S2 in the Supporting Information) and Figure 6, indicate:

1) Rotation of the internal Sc_3N unit is more hindered once the fullerene is exohedrally functionalized, as found for Diels–Alder and other derivatives of I_h-C_{80}.[12,13]
2) As observed by Campanera et al. for I_h-C_{80} and by Osuna et al. for D_{3h}-C_{78},[9,18] the reaction energies are less exothermic than for the addition onto the pristine D_{5h}-C_{80} cage.
3) In general, the difference between the reaction energies over the nonequivalent bonds, that is, the regioselectivity, is reduced.
4) Interestingly, two [5,6] bonds, ***D*$_{5h}$-b** and ***D*$_{5h}$-c**, remain the most reactive bonds. Due to their relative energy with respect to other regioisomers (around 5 kcal mol^{-1}), these two adducts should be the most abundant products under thermodynamic control. This is in contrast to the results observed for $Sc_3N@D_{3h}$-C_{78} in which the most stable adduct is one of the [6,6] B adducts. The difference in exothermicity of the reaction over bonds ***D*$_{5h}$-b** and ***D*$_{5h}$-c** is now reduced to less than 2 kcal mol^{-1}.
5) Bond **3**, of [6,6] B type, yields the third most stable adduct. This bond, which is one of the less reactive bonds in the pristine cage, is activated by the presence of the nitride cluster.
6) The pyracylenic bond ***D*$_{5h}$-5**, which is the most reactive [6,6] bond in the hollow fullerene, is now rather deactivated. Bond ***D*$_{5h}$-2**, also of [6,6] B type, is more reactive than ***D*$_{5h}$-5**.
7) The orientational isomers in which two Sc atoms are pointing to the two sides of the functionalized bond (see Figure 4 and 5) are usually the most stable isomers for [5,6] bonds, similarly to what happens in the pyrrolidine adducts of $Sc_3N@I_h$-C_{80}. For the most stable [6,6] adducts (bonds ***D*$_{5h}$-2** and ***D*$_{5h}$-3**), orientational isomer 5 is the one with the lowest energy in good agreement with the results of the Prato reaction on $Sc_3N@I_h$-C_{80}.[13]

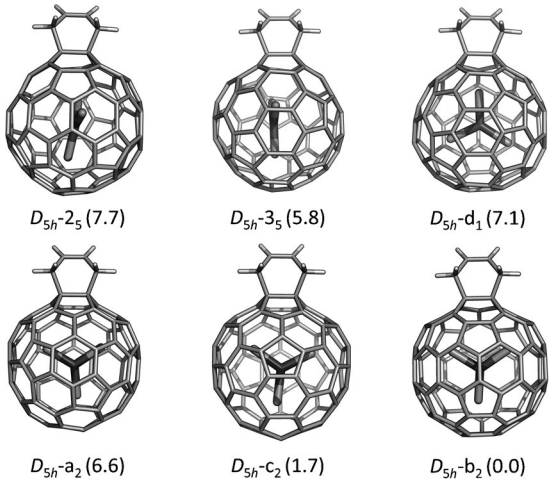

Figure 5. Representation of the six lowest-energy regioisomers for the Diels–Alder cycloaddition between s-*cis*-1,3-butadiene and $Sc_3N@D_{5h}$-C_{80}. The different regioisomers are named according to nomenclature described in Figure 2. For example, ***D*$_{5h}$-2$_x$** is the adduct on bond 2, for which ***x*** denotes the orientation of the metal nitride. Only the lowest-energy orientation of nitride is shown. In parenthesis, the relative energies [kcal mol^{-1}] with respect to the lowest-energy ***D*$_{5h}$-b$_2$** isomer. All the computed adducts can be found in the Supporting Information.

Based on the results shown so far, $Sc_3N@I_h$-C_{80} is somewhat more reactive than $Sc_3N@D_{5h}$-C_{80} from the thermodynamic point of view, that is, from the exothermicity of the addition reactions. The two isomers are also more reactive than $Sc_3N@D_{3h}$-C_{78}.[18]

Energy barriers for Diels–Alder cycloaddition on $Sc_3N@I_h$-C_{80} and $Sc_3N@D_{5h}$-C_{80}: Transition-state (TS) structures for each of the nonequivalent bonds of the empty cages I_h-C_{80} and D_{5h}-C_{80} as well as the endohedral fullerenes $Sc_3N@I_h$-C_{80} and $Sc_3N@D_{5h}$-C_{80} were computed. In all cases, the TS search started from a symmetric structure in which the two C–C bonds to be formed have the same bond length, thus leading, in most cases, to an asynchronous TS (even in the symmetric addition sites, at which the synchronous TS is actually a second-order saddle point).[41]

Isomer I_h: In the case of the hollow I_h-C_{80} cage, the product under kinetic control, that is, the one with the lowest-energy activation barrier, does not correspond to the product under

thermodynamic control, as the lowest barrier is found for the addition of the diene to a [6,6] bond (***I_h*-1**, $\Delta E^{\neq}$ = 2.9 kcal mol^{-1}; Table 1). The TS for the cycloaddition to the [5,6] bond presents a slightly higher activation barrier (***I_h*-a**, $\Delta E^{\neq}$ = 3.8 kcal mol^{-1}). For the metallofullerene $Sc_3N@I_h$-C_{80}, the lowest activation barrier is obtained for the regioisomer that presents the most exothermic reaction energy (***I_h*-a$_6$**, 15.7 kcal mol^{-1}; Table 2). The differences in $\Delta E^{\neq}$ between [6,6] and [5,6] additions are larger than in hollow I_h-C_{80}. The changes in the reaction barriers for different orientations of the metal nitride are smaller than the changes found in the reaction energies (Table S3 in the Supporting Information). For example, the transition states for ***I_h*-a$_2$** and ***I_h*-a$_7$** are only 0.3 and 1.6 kcal mol^{-1} higher in energy than that of ***I_h*-a$_6$**, respectively. The rest of the [5,6] orientational isomers in which the metal nitride is either faced or situated perpendicularly to the attacked bond present higher activation barriers (19.7–21.3 kcal mol^{-1}). These higher reaction barriers are mainly attributed to higher deformation energies of both the cage and the diene (Table S5 in the Supporting Information). It is important to note that the internal cluster adapts its position along the reaction to minimize the activation barrier. The mobility of the cluster decreases significantly in the region of the potential-energy surface close to the product.

Isomer D_{5h}: Table 1 also displays the reaction barriers and C−C bond lengths that are being formed at the TS for the hollow D_{5h}-C_{80} cage. The barriers are significantly larger than for the I_h-C_{80} isomer and smaller than those found for the D_{3h}-C_{78} cage. This concurs with the fact that the free D_{5h} cage is approximately 11 kcal mol^{-1} more stable than the I_h-C_{80} isomer. The lowest barrier corresponds to bonds ***D_{5h}*-4** and ***D_{5h}*-b** (7.1 and 8.1 kcal mol^{-1}, respectively) followed by bonds ***D_{5h}*-2**, ***D_{5h}*-c**, ***D_{5h}*-5**, and ***D_{5h}*-3** with barriers that are up to 3 kcal mol^{-1} larger. Bonds ***D_{5h}*-d**, ***D_{5h}*-a**, and ***D_{5h}*-1** show even larger barriers, especially the last two with values larger than 15 kcal mol^{-1}. It is interesting to point out that the adduct on bond ***D_{5h}*-b** is the thermodynamic as well as one of the kinetically preferred products (second-lowest barrier). Bond ***D_{5h}*-4**, which yields an adduct that is not very stable, is very reactive kinetically speaking (lowest barrier). It is also interesting to point out that the lowest-energy adduct on a [6,6] bond (***D_{5h}*-5**, pyracylenic bond) displays a relatively low barrier. The largest barrier is observed for bond ***D_{5h}*-1**, which is also predicted to have the most endothermic reaction energy. Most of the TS are highly asynchronous except for ***D_{5h}*-a** and ***D_{5h}*-5**, which show similar C···C distances for the bonds that are being formed.

For the Diels–Alder reaction between $Sc_3N@D_{5h}$-C_{80} and s-*cis*-1,3-butadiene, we have only computed the TS for the most stable orientational isomers for each of the regioisomers (Table 2). All the computed barriers are larger than those found for the empty D_{5h}-C_{80} cage. This reduced reactivity for the EMF relative to the hollow cage has been also observed for the I_h-C_{80} and D_{3h}-C_{78} systems, and it is easily understood by comparing the HOMO–LUMO gaps of the different species (i.e., 0.130, 1.516 eV for I_h-C_{80} and $Sc_3N@I_h$-C_{80}; and 0.084 and 1.114 eV for D_{5h}-C_{80} and $Sc_3N@D_{5h}$-C_{80}, respectively). The lowest barrier is now found for bond ***D_{5h}*-b** (13.4 kcal mol^{-1}). The barriers for the other regioisomers are more than 2.5 kcal mol^{-1} larger. The second-lowest barrier corresponds to bond ***D_{5h}*-3** (16.2 kcal mol^{-1}), the third most stable product. The second most stable regioisomer, the adduct on bond ***D_{5h}*-c**, features a barrier that is almost 4 kcal mol^{-1} larger than for the adduct on bond ***D_{5h}*-b**. The barriers for the other regioisomers are larger, especially for bonds ***D_{5h}*-4** and ***D_{5h}*-5** (almost 22 kcal mol^{-1}). Bond ***D_{5h}*-4**, which is one of the two most reactive bonds in the hollow fullerene from the kinetic point of view, is importantly deactivated once the Sc_3N is encapsulated. All TS except two are found to be very asynchronous. In general, the orientation of the nitride cluster does not affect the barriers as much as the energies of the final products.

After these computations, regioisomer ***D_{5h}*-b** of [5,6] type B, is predicted to be the thermodynamic as well as the kinetic product. It is important to note that the TS for the adduct on bond ***D_{5h}*-5**, the [6,6] pyracylenic bond, lies more than 8 kcal mol^{-1} higher than the lowest barrier (bond ***D_{5h}*-b**). Therefore, this bond does not seem to be the most reactive one from the kinetic point of view in contrast to the predictions done by Dorn and co-workers from NMR spectroscopic experiments.[14] In a recent study, we have reported the reaction energies as well as the NMR spectroscopic chemical shifts computed at the KT2/ET-pVQZ level for the *N*-trityl-pyrrolidino mono-adducts of $Sc_3N@D_{5h}$-C_{80}. These calculations showed that indeed the preferred addition for the 1,3-dipolar functionalization of the nitride EMF corresponds to the ***D_{5h}*-b$_2$** bond, which exhibits moreover a NMR pattern that is consistent with the data by Dorn et al.[42]

Comparison of the activation barriers for the two $Sc_3N@C_{80}$ isomers (Table 2 and Figures 6 and 7) shows that $Sc_3N@D_{5h}$-C_{80} should exhibit higher reactivity, that is, react faster than the I_h isomer towards the diene under the Diels–Alder cycloaddition, as observed recently by Dorn and co-workers.[14] This observation is also consistent with the smaller HOMO–LUMO gap for $Sc_3N@D_{5h}$-C_{80} (1.516 and 1.114 eV for the Sc-based I_h- and D_{5h}-C_{80} cages, respectively) and the higher deformation energy of the D_{5h} cage (the deformation energies that correspond to the nitride cluster encapsulation are 18.2 and 15.8 kcal mol^{-1} for $Sc_3N@D_{5h}$-C_{80} and $Sc_3N@I_h$-C_{80}, respectively).

Effect of the metal nitride: Diels–Alder cycloaddition on $M_3N@I_h$-C_{80} and $M_3N@D_{5h}$-C_{80} (M=Lu and Gd): We have extended our study to investigate the exohedral reactivity of some (bio)chemically important nitride metallofullerenes that contain Lu_3N and Gd_3N instead of Sc_3N to analyze the influence of the metal on this type of reactions. As already pointed out previously, the metal nitride is easily rotated in $Sc_3N@I_h$-C_{80}.[38] The ^{13}C NMR spectrum at ambient temperature of $Lu_3N@I_h$-C_{80} confirmed that there exists a motional averaging of the Lu_3N similar to that of Sc_3N in $Sc_3N@I_h$-C_{80}.[43] Moreover, some of us previously studied the differ-

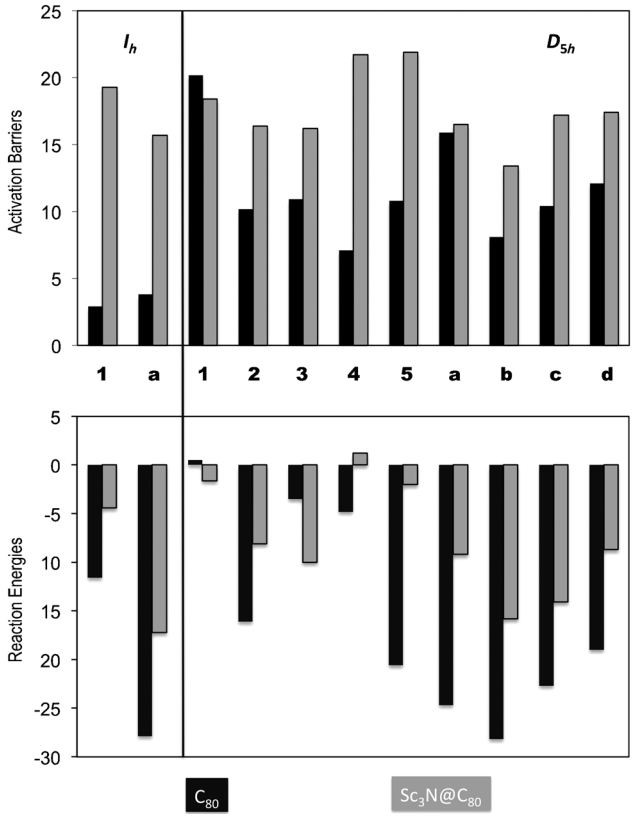

Figure 6. Comparison of the reaction energies and activation barriers [kcal mol^{-1}] found for the Diels–Alder reaction over the nonequivalent bonds of the hollow I_h and D_{5h} cages (black) and the EMFs $Sc_3N@I_h$-C_{80} and $Sc_3N@D_{5h}$-C_{80} (gray). Reaction energies and barriers are shown only for the lowest-energy orientations of the metal nitride.

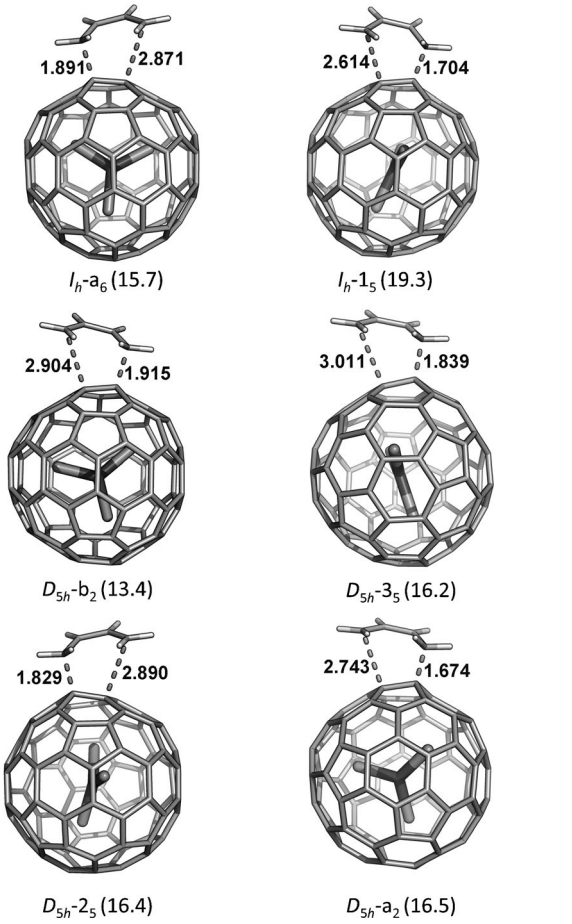

Figure 7. Representation of the TS structures for the Diels–Alder cycloaddition between s-*cis*-1,3-butadiene and $Sc_3N@I_h$-C_{80} or $Sc_3N@D_{5h}$-C_{80}. All the computed TS structures can be found in the Supporting Information.

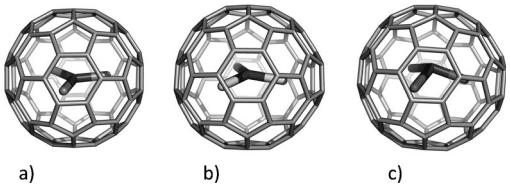

Figure 8. Representation of the endohedral metallofullerenes: a) $Sc_3N@I_h$-C_{80}, b) $Lu_3N@I_h$-C_{80}, and c) $Gd_3N@I_h$-C_{80}. In the latter compound, the nitrogen atom is displaced out of the Gd_3 plane.

ence in energy between the orientational isomers at BP86/TZP for $Y_3N@I_h$-C_{80} and found rather small energy differences (less than 3 kcal mol^{-1}).[44] We note here that Lu^{3+} is slightly smaller than Y^{3+} (their ionic radii are 100 and 104 pm, respectively).[45] In light of the experimental and theoretical observations that the Lu_3N unit is also easily rotated, we have employed the same procedure as for $Sc_3N@I_h$-C_{80}. Therefore, we have studied the cycloaddition reaction over the two nonequivalent bonds and considered different orientations of the Lu_3N moiety. The rotation of the larger Gd_3N is more debatable. It was proposed from Raman spectra that the free cluster rotation is prevented in $Gd_3N@I_h$-C_{80} due to the interaction between the Gd_3N cluster and the C_{80} cage.[46] In contrast, a recent study showed that the energy differences between the different orientational isomers of $Gd_3N@I_h$-C_{80} are very low (less than 2 kcal mol^{-1}).[44] To allow a full comparison between all analyzed systems, we decided to investigate the exohedral reactivity of $Gd_3N@I_h$-C_{80} as in the other two studied cases considering the reaction over the [5,6] and [6,6] bonds with different orientations of the Gd_3N unit. The same analysis was done for $M_3N@D_{5h}$-C_{80} (M = Lu, Gd; Figure 8).

Reaction energies: In Table 3, the reaction energies for the Diels–Alder reaction over the different [5,6] and [6,6] bonds with the different Lu_3N orientations are shown. The preferred addition site in the case of $Lu_3N@I_h$-C_{80} corresponds to the [5,6] $\boldsymbol{I_h}$**-a** bond, as found also for M = Sc. Again, the lowest-energy orientational isomers present the metal cluster situated in the same plane as the attacked bond but with the Lu atoms situated far away from it ($\boldsymbol{I_h}$**-a$_2$** and $\boldsymbol{I_h}$**-a$_6$** with reaction energies of −13.1 and −14.5 kcal mol^{-1}, respectively; Table S6 in the Supporting Information). Therefore, the change of the Sc_3N inner cluster for Lu_3N does not affect the regioselectivity of the Diels–Alder cycloaddition on the cage. It is important to note that the third most exothermic reaction energy is obtained for the isomer $\boldsymbol{I_h}$**-a$_3$**, which has

Table 3. Reaction energies and bond lengths in the lowest-energy final products of the Diels–Alder addition on the EMFs $Lu_3N@I_h$-C_{80} and $Lu_3N@D_{5h}$-C_{80}.[a–c]

Bond	Bond type[b]	ΔE_R	R_{full}	R_{CC}	
$Lu_3N@I_h$-C_{80}					
$\boldsymbol{I_h}$-$\mathbf{a_6}$	D [5,6]	−14.5	1.641	1.559	1.558
$\boldsymbol{I_h}$-$\mathbf{1_3}$	B [6,6]	−7.1	1.702	1.563	1.562
$Lu_3N@D_{5h}$-C_{80}					
$\boldsymbol{D_{5h}}$-$\mathbf{b_2}$	D [5,6]	−15.9	1.648	1.562	1.563
$\boldsymbol{D_{5h}}$-$\mathbf{d_1}$	D [5,6]	−14.0	1.680	1.559	1.559
$\boldsymbol{D_{5h}}$-$\mathbf{c_2}$	D [5,6]	−11.7	1.664	1.565	1.562
$\boldsymbol{D_{5h}}$-$\mathbf{3_1}$	B [6,6]	−10.8	1.705	1.562	1.562
$\boldsymbol{D_{5h}}$-$\mathbf{2_5}$	B [6,6]	−9.5	1.589	1.577	1.578
$\boldsymbol{D_{5h}}$-$\mathbf{a_2}$	D [5,6]	−8.4	1.655	1.567	1.567
$\boldsymbol{D_{5h}}$-$\mathbf{4_1}$	B [6,6]	−7.6	1.708	1.562	1.566
$\boldsymbol{D_{5h}}$-$\mathbf{1_1}$	C [6,6]	−4.5	1.883	1.554	1.553
$\boldsymbol{D_{5h}}$-$\mathbf{5_1}$	A [6,6]	−1.8	1.623	1.574	1.567

[a] Reaction energies, ΔE_R [kcal mol^{-1}] and bond lengths [Å]; R_{full} is the length of the C–C bond over which the reaction took place, and R_{CC} are the bond lengths of the two newly formed C–C bonds. [b] Bond-type classification according to Figure 1. [c] Only the lowest-energy orientational isomer for each regioisomer is shown. The complete table with all the studied adducts can be found in the Supporting Information.

one of the lutetium atoms in close contact with the attacked [5,6] bond ($\Delta E_R = -10.2$ kcal mol^{-1}; see Table S6 in the Supporting Information). Actually, the isomers $\boldsymbol{I_h}$-$\mathbf{a_1}$, $\boldsymbol{I_h}$-$\mathbf{a_3}$, and $\boldsymbol{I_h}$-$\mathbf{a_4}$ present one of the lutetium atoms facing the attacked bond and their reaction energies are substantially exothermic (they range from −9.1 to −10.2 kcal mol^{-1}; see Table S6 in the Supporting Information). Therefore, the encapsulation of larger metal nitrides produces an increase in the reactivity of those bonds that present one of the metal atoms in close contact (see Figure 9). Certainly, this preference is not unexpected. It was found that the exohedral reactivity of endohedral metallofullerenes that encapsulate large nitride units is led by the fullerene strain energy.[19,47] In fact, the deformation energy of the I_h-C_{80} fullerene cage for encapsulating Lu_3N is 11.0 kcal mol^{-1} higher than for Sc_3N (the deformation energies are 15.8 and 26.8 kcal mol^{-1} for $Sc_3N@I_h$-C_{80} and $Lu_3N@I_h$-C_{80}). The exohedral functionalization through those bonds situated close to one of the metal atoms of the nitride leads to a less strained situation in which the pyramidalization of the attacked carbon bonds gives extra space to the nitride unit. It is therefore not surprising that the reaction energies for the isomers $\boldsymbol{I_h}$-$\mathbf{a_5}$ and $\boldsymbol{I_h}$-$\mathbf{a_8}$, which present the Lu_3N perpendicular to the attacked [5,6] bond, have low exothermicities (the reaction energies are −1.0 and −2.2 kcal mol^{-1}, respectively). As it so happens with the scandium-based related compound, the cycloaddition to [6,6] bonds is less favorable. The most stable [6,6] isomer corresponds to $\boldsymbol{I_h}$-$\mathbf{1_3}$ (reaction energy of −7.1 kcal mol^{-1}), with the nitride directly facing again the attacked [6,6] bond. Other orientational isomers with the Lu atoms far from the [6,6] bond present substantially less exothermic reaction energies (from −0.3 to −1.7 kcal mol^{-1}; Table S6 in the Supporting Information).

For the reaction on $Lu_3N@D_{5h}$-C_{80}, no significant changes are found relative to $Sc_3N@D_{5h}$-C_{80}. Although the deformation energy of the D_{5h}-C_{80} cage for encapsulating Lu_3N is substantially higher than for Sc_3N (18.2 and 31.5 kcal mol^{-1}, respectively), the similar reactivity of the two compounds might be attributed to the slightly larger HOMO–LUMO gap for $Lu_3N@D_{5h}$-C_{80} than for $Sc_3N@D_{5h}$-C_{80} (1.314 and 1.114 eV, respectively). We have only analyzed the lowest-energy orientational isomers for each of the regioisomers (a total of twenty one isomers; Table S7 in the Supporting Information). The most stable regioisomer is also the adduct formed on bond $\boldsymbol{D_{5h}}$-**b**, the reaction energy being almost the same as for the Sc derivative. The second most stable regioisomer corresponds now to the adduct on bond $\boldsymbol{D_{5h}}$-**d**, which lies only less than 2 kcal mol^{-1} higher than the adduct on bond $\boldsymbol{D_{5h}}$-**b** and which is more stable than adducts on bonds $\boldsymbol{D_{5h}}$-**c**, $\boldsymbol{D_{5h}}$-**3**, and $\boldsymbol{D_{5h}}$-**a** in contrast to what happens in the Sc_3N EMF. As for the I_h cage, those orientations in which the metal atom is pointing to the functionalized bond, $\boldsymbol{D_{5h}}$-$\mathbf{d_1}$, become more favored as long as the metal in the cluster is larger.[13] Indeed, important stabilizations of orientational isomer **1** are found for all the regioisomers with reaction energies that become between 3.4 (bond $\boldsymbol{D_{5h}}$-**c**) and

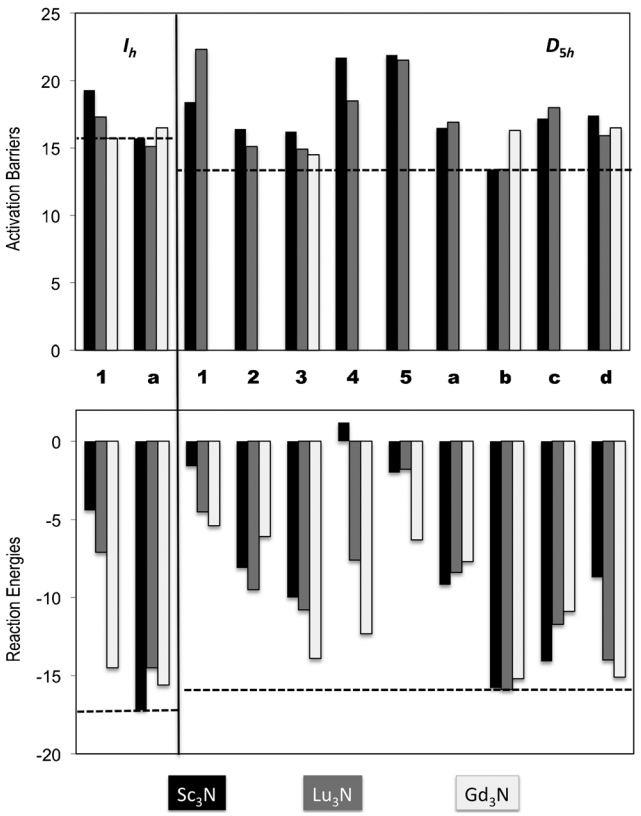

Figure 9. Comparison of the reaction energies and activation barriers [kcal mol^{-1}] found for the Diels–Alder reaction over the nonequivalent bonds of $M_3N@I_h$-C_{80} and $M_3N@D_{5h}$-C_{80} (M = Sc, black; Lu, gray; Gd, white). Only energies for the lowest-energy orientations of the metal nitride are considered. Broken lines compare the lowest reaction energies and activation barriers for the I_h and D_{5h} isomers of $Sc_3N@C_{80}$, showing a smaller barrier, that is, higher reactivity, for the D_{5h} isomer in good agreement with the experiments.[14]

16.9 (bond D_{5h}-**1**) kcal mol^{-1} more exothermic now in the case of the Lu-EMF than in the Sc nitride. Bond D_{5h}-**5** leads to the least stable adduct among all the regioisomers that we have computed with a reaction energy very similar to that found for the Sc EMF.

The exploration of the chemical reactivity of the gadolinium nitride metallofullerene $Gd_3N@I_h$-C_{80} draws interesting results. In contrast with $Sc_3N@I_h$-C_{80} and $Lu_3N@I_h$-C_{80}, the Diels–Alder reaction is favored over both [5,6] and [6,6] bonds and there are six isomers (I_h-**1**$_1$, I_h-**a**$_1$, I_h-**a**$_2$, I_h-**a**$_3$, I_h-**a**$_4$, and I_h-**a**$_6$) that present favorable reaction energies that range from −14.1 to −15.6 kcal mol^{-1} (Table 4 and Table S8 in the Supporting Information). This lower regioselectivity is mainly attributed to the higher deformation energy of the fullerene cage. The I_h-C_{80} cage is more distorted when the larger Gd_3N unit is encapsulated inside (the deformation energy is 31.8 kcal mol^{-1}, that is, 16 kcal mol^{-1} larger than for Sc_3N). Of course, the higher the deformation energy of the cage the more reactive the fullerene structure as the strain is partially released after the reaction. Those isomers that display significant negative reaction energies present the Gd_3N cluster either faced or situated far away from the attacked bond, but as a general rule the nitride unit and the C–C bond that has the diene attached are contained in the same plane (Table S8 in the Supporting Information).

For $Gd_3N@D_{5h}$-C_{80}, the lowest-energy regioisomer is still the adduct on bond D_{5h}-**b**, the reaction energy being almost the same as for the other metal clusters (within 1 kcal mol^{-1}; Table 4). Other regioisomers with the Gd_3N cluster oriented with a Gd ion pointing towards the functionalized bond are now almost as stable as adduct D_{5h}-**b**$_2$, especially isomer D_{5h}-**d**$_1$. In general, the reaction energies are more exothermic (see Table 4 and Table S9 in the Supporting Information). As in the icosahedral isomer, regioselectivity is significantly reduced relative to M = Lu and Sc.

Reaction barriers: Finally, we analyzed the kinetics of the addition of s-*cis*-1,3-butadiene to $Lu_3N@C_{80}$ and $Gd_3N@C_{80}$. In the latter case and due to the high computational cost of the present calculations, we located the transition states that correspond to the three preferred addition sites. This is in part justified by the fact that the kinetic and thermodynamic products coincide in most cases (see above). In Tables 5 and 6, the activation barriers for the Lu- and Gd-based metallofullerenes are presented.

Table 4. Reaction energies and bond lengths in the lowest-energy final products of the Diels–Alder addition on the EMFs $Gd_3N@I_h$-C_{80} and $Gd_3N@D_{5h}$-C_{80}.[a–c]

Bond	Bond type[b]	ΔE_R	R_{full}	R_{CC}	
$Gd_3N@I_h$-C_{80}					
I_h-**a**$_2$	D [5,6]	−15.6	1.652	1.557	1.557
I_h-**1**$_1$	B [6,6]	−14.5	1.710	1.563	1.559
$Gd_3N@D_{5h}$-C_{80}					
D_{5h}-**b**$_2$	D [5,6]	−15.2	1.655	1.556	1.557
D_{5h}-**d**$_1$	D [5,6]	−15.1	1.697	1.554	1.552
D_{5h}-**3**$_1$	B [6,6]	−13.9	1.727	1.556	1.557
D_{5h}-**4**$_1$	B [6,6]	−12.3	1.730	1.556	1.556
D_{5h}-**c**$_2$	D [5,6]	−10.9	1.679	1.556	1.559
D_{5h}-**a**$_2$	D [5,6]	−7.7	1.659	1.560	1.560
D_{5h}-**5**$_1$	A [6,6]	−6.3	1.635	1.566	1.563
D_{5h}-**2**$_5$	B [6,6]	−6.1	1.593	1.576	1.573
D_{5h}-**1**$_1$	C [6,6]	−5.4	2.055	1.541	1.539

[a] Reaction energies, ΔE_R [kcal mol^{-1}] and bond lengths [Å], R_{full} is the length of the C–C bond over which the reaction took place, and R_{CC} are the bond lengths of the two newly formed C–C bonds. [b] Bond-type classification according to Figure 1. [c] Only the lowest-energy orientational isomer for each regioisomer is shown. The complete table with all the studied adducts can be found in the Supporting Information.

Table 5. Reaction barriers and lengths for the C–C bonds being formed at the transition state for the EMFs $Lu_3N@I_h$-C_{80} and $Lu_3N@D_{5h}$-C_{80}.[a–c]

Bond	Bond type[b]	TS	$\Delta E^{\neq}$	R_{CC}	
$Lu_3N@I_h$-C_{80}					
I_h-**a**$_6$	D [5,6]	asyn	15.1	1.872	2.903
I_h-**1**$_3$	B [6,6]	asyn	17.3	1.958	2.418
$Lu_3N@D_{5h}$-C_{80}					
D_{5h}-**b**$_2$	D [5,6]	asyn	13.4	1.889	2.946
D_{5h}-**3**$_5$	B [6,6]	asyn	14.9	1.723	2.921
D_{5h}-**2**$_5$	B [6,6]	asyn	15.1	1.735	2.794
D_{5h}-**d**$_1$	D [5,6]	asyn	15.9	2.027	2.424
D_{5h}-**a**$_2$	D [5,6]	asyn	16.9	1.660	2.602
D_{5h}-**c**$_2$	D [5,6]	asyn	18.0	1.873	2.735
D_{5h}-**4**$_1$	B [6,6]	asyn	18.5	1.929	2.427
D_{5h}-**5**$_8$	A [6,6]	asyn	21.5	1.942	2.409
D_{5h}-**1**$_5$	C [6,6]	asyn	22.1	1.681	2.521

[a] Reaction barriers ($\Delta E^{\neq}$) [kcal mol^{-1}] and bond lengths (R_{CC}) [Å]. [b] Bond-type classification according to Figure 1. [c] Only the lowest-energy orientational isomer for each TS is shown. The complete table with all the studied TS can be found in the Supporting Information.

Table 6. Reaction barriers and lengths for the C–C bonds being formed at the transition state for the EMFs $Gd_3N@I_h$-C_{80} and $Gd_3N@D_{5h}$-C_{80}.[a–c]

Bond	Bond type[b]	TS	$\Delta E^{\neq}$	R_{CC}	
$Gd_3N@I_h$-C_{80}					
I_h-**1**$_1$	B [6,6]	asyn	15.7	1.951	2.546
I_h-**1**$_3$	B [6,6]	asyn	15.7	1.935	2.552
I_h-**a**$_4$	D [5,6]	asyn	16.5	1.939	2.512
$Gd_3N@D_{5h}$-C_{80}					
D_{5h}-**3**$_5$	B [6,6]	asyn	14.5	1.849	3.074
D_{5h}-**b**$_2$	D [5,6]	asyn	16.3	1.879	2.898
D_{5h}-**d**$_1$	D [5,6]	asyn	16.5	2.024	2.445

[a] Reaction barriers ($\Delta E^{\neq}$) [kcal mol^{-1}] and bond lengths (R_{CC}) [Å]. [b] Bond-type classification according to Figure 1. [c] Only the lowest-energy orientational isomer for each TS is shown. The complete table with all the studied TS can be found in the Supporting Information.

For $Lu_3N@I_h$-C_{80}, the product under kinetic control is the same as the product under thermodynamic control, the [5,6] regioisomer I_h-**a**$_6$, as is the case for $Sc_3N@I_h$-C_{80} (Tables 3 and 5). This cycloaddition product has the lowest activation barrier (15.1 kcal mol^{-1}) among all considered cases. It is interesting to note here that the lowest reaction barrier obtained for the Sc metallofullerene is 0.6 kcal mol^{-1} higher in energy than for the Lu compound. Other orientational iso-

mers with the cluster placed far away from the attacked bond (***I*$_h$-a$_2$**) or with one of the Lu atoms directly facing it (***I*$_h$-a$_4$**, ***I*$_h$-a$_1$**, ***I*$_h$-a$_3$**) show activation barriers that are slightly larger (within 1 kcal mol^{-1}; Table S10 in the Supporting Information). As already observed for the reaction energies, there is an increase in the reactivity for those regioisomers that present the Lu atoms situated close to the C–C bond at which the cycloaddition reaction is being performed. The transition states that lead to the [6,6] addition present activation barriers that range from 17.3 to 21.8 kcal mol^{-1}. Therefore, as it so happens for $Sc_3N@I_h$-C_{80}, the cycloaddition reaction on [6,6] bonds is less favored.

For $Lu_3N@D_{5h}$-C_{80}, very similar results are obtained relative to the Sc-based endohedral. The lowest barriers correspond to two orientational isomers of the regioisomer on bond ***D*$_{5h}$-b**, analogously as in $Sc_3N@D_{5h}$-C_{80}, the reaction barriers being the same (within tenths of kcal mol^{-1}; Table S11 in the Supporting Information). Barriers for the adducts on bonds ***D*$_{5h}$-2** and ***D*$_{5h}$-3**, which are now around 15 kcal mol^{-1}, are slightly reduced (1 kcal mol^{-1}) as it occurs for the barriers for regioisomers ***D*$_{5h}$-d** and ***D*$_{5h}$-a**. The most significant reduction (3.2 kcal mol^{-1}) is observed for the barrier of the adduct on bond ***D*$_{5h}$-4**, which is in line with the important stabilization of the final product. The barrier for regioisomer ***D*$_{5h}$-5** does not change appreciably. It is interesting to remark here that our predictions about the reaction barriers in the two isomers of $Lu_3N@C_{80}$ are in agreement with the experimental fact that $Lu_3N@D_{5h}$-C_{80} exhibits higher reactivity with respect to dienes than the $Lu_3N@I_h$-C_{80} isomer.[14] Both $Lu_3N@D_{5h}$-C_{80} and $Lu_3N@I_h$-C_{80} present LUMOs of similar energy, so that the $HOMO_{diene}$–$LUMO_{dienophile}$ gap is almost identical. Again, the higher reactivity of the lutetium-based D_{5h} cage is attributed to the smaller HOMO–LUMO gap of the D_{5h} compound (1.314 and 1.625 eV for $Lu_3N@D_{5h}$-C_{80} and $Lu_3N@I_h$-C_{80}, respectively) and the higher deformation energy of the D_{5h} cage for encapsulating the Lu_3N unit (31.5 and 26.8 kcal mol^{-1}, respectively).

As mentioned before, we have located the TS for $Gd_3N@I_h$-C_{80}, but only for those regioisomers that presented the most exothermic reaction energies (Table S12 in the Supporting Information). Interestingly, the product under kinetic control is not the same as the one under thermodynamic control. The preferred regioisomer from the thermodynamic point of view is the [5,6] ***I*$_h$-a$_2$** (the reaction energy is −15.6 kcal mol^{-1}). However, the isomers that present the lowest activation barrier correspond to addition to the [6,6] bond, ***I*$_h$-1$_1$** and ***I*$_h$-1$_3$** (with the same reaction barrier of 15.7 kcal mol^{-1}). Instead, the activation barrier for the thermodynamic regioisomer ***I*$_h$-a$_2$** is 16.7 kcal mol^{-1}. Other orientations of the cluster lead to very similar activation barriers (within 1 kcal mol^{-1}; Table S12 in the Supporting Information).

In a previous combined experimental/theoretical study, the regioselectivity of the 1,3-dipolar cycloaddition reaction was compared for the mixed species $Sc_xGd_{3-x}N@I_h$-C_{80} (x = 0–3).[48] Experiments showed that the regioselectivity of the reaction was drastically changed as the [5,6] regioisomer was obtained in the case of $Sc_3N@I_h$-C_{80}, whereas for $Gd_3N@I_h$-C_{80} it was the [6,6] one. Chen et al. computed the difference in stability between the [5,6] and [6,6] regioisomers at the Perdew–Burke–Ernzerhof/double-numeric-polarized (PBE/DNP) level and observed that for Sc the [5,6] adduct was favored by 11.7 kcal mol^{-1}, whereas for Gd it was the [6,6] one by 0.4 kcal mol^{-1}. They found a very low difference in energy between both additions for $Gd_3N@I_h$-C_{80}, which indeed concurs with our computed reaction energies (although we found that the [5,6] regioisomer is somewhat lower in energy than the [6,6] one). Our calculations indicate that the difference in reactivity observed experimentally must be essentially due to the lower activation barrier found for the [6,6] addition. An exploration of the kinetics of the Diels–Alder reaction on $Gd_3N@I_h$-C_{80} is therefore crucial to fully understand the experimental findings.

With regards to $Gd_3N@D_{5h}$-C_{80}, we have also computed the TS for only the three lowest-energy regioisomers. Interestingly, we have found that the lowest barrier among those that we have computed does not correspond to adduct ***D*$_{5h}$-b$_2$**, but to a [6,6]-type bond (***D*$_{5h}$-3$_5$**). Therefore, orientation **1** of the cluster, which favors the products, does not favor the TS as much. The energy barrier is somewhat larger than for M = Sc and Lu (13.4 kcal mol^{-1} for these two metals). As a characteristic difference relative to smaller and less electropositive metals, we find that for Gd_3N the thermodynamic product is different from the kinetic product, as occurs for the I_h-C_{80} isomer.

Conclusion

We have performed a thorough computational study of the Diels–Alder reaction on the two cage isomers (I_h and D_{5h}) of $M_3N@C_{80}$ for M = Sc, Lu, and Gd. We have analyzed the effect of addition of s-*cis*-1,3-butadiene on the different C–C bonds of each carbon cage. Due to the observed rotation of the nitride cluster inside the carbon cages, several orientations of the nitride have been taken into consideration and therefore an exhaustive search of all relevant stationary points in the potential-energy surface has been necessary.

As observed in $Sc_3N@C_{78}$, all the endohedral species are less reactive than their homologous hollow cages. When the Sc_3N is encapsulated inside the icosahedral cage, the [5,6] adduct is more stable than the [6,6] one by more than 12 kcal mol^{-1}. The energy difference between the corresponding TS, however, is notably smaller (4 kcal mol^{-1}). For the less-symmetric D_{5h} cage, we have explored the reactivity of all nine distinct bonds. The regioisomer proposed from the ^{1}H NMR spectra to be the product under thermodynamic control for the Prato cycloaddition, the adduct on the [6,6] pyracylenic bond ***D*$_{5h}$-5**, is not found among the lowest-energy regioisomers and shows one of the larger reaction barriers. From our work, we propose regioisomer ***D*$_{5h}$-b** to be the product under thermodynamic control for the Diels–Alder cycloaddition on $Sc_3N@D_{5h}$-C_{80}. Bond ***D*$_{5h}$-b**, which is

the most similar to the unique [5,6] bond type in the icosahedral cage, is the most reactive bond. The activation barrier computed for this bond is 13.4 kcal mol^{-1}, 2.3 kcal mol^{-1} lower than the barrier for the ***I_h*-a** bond, which is in excellent agreement with the experiments.

The reactivity of $Lu_3N@C_{80}$ is rather similar to that of the scandium nitride homologues, although the regioselectivity is somewhat smaller for both I_h and D_{5h} cages. The situation is rather different for the larger and more electropositive Gd^{3+} ion. Once the cage is functionalized, the M_3N unit (M = Sc, Lu) tends to orient in such a way that the M atoms do not directly point to the functionalized C–C bond, rather the nitride and the bond are coplanar. Those orientations with one M atom pointing to the functionalized bond result in an increase in stability for larger and more electropositive metals. The size of Lu is not enough to reverse the relative stability of the above-mentioned orientational isomers, but for Gd, some [6,6] regioisomers that contain nitrides with the metal pointing towards the attacked bond become competitive. Calculations also show that for $Gd_3N@I_h$-C_{80} and $Gd_3N@D_{5h}$-C_{80} the product under kinetic control is not the same as the one under thermodynamic control.

Acknowledgements

The following organizations are thanked for financial support: the Ministerio de Ciencia e Innovación (MICINN; project numbers CTQ2008-06532/BQU, CTQ2008-06549-C02-01/BQU, CTQ2011-23156/BQU, and CTQ2011-25086/BQU), the DIUE of the Generalitat de Catalunya (project numbers 2009SGR637, 2009SGR528, 2009SGR462, and XRQTC), and the European Community (postdoctoral fellowship PIOF-GA-2009-252856). Excellent service by the Centre de Serveis Científics i Acadèmics de Catalunya (CESCA) is gratefully acknowledged. The authors are also grateful to the computer resources, technical expertise, and assistance provided by the Barcelona Supercomputing Center - Centro Nacional de Supercomputación. Support for the research of M. Solà was received through the ICREA Academia 2009 prize for excellence in research funded by the DIUE of the Generalitat de Catalunya.

[1] a) *Endofullerenes: A New Family of Carbon Clusters* (Eds.: T. Akasaka, S. Nagase), Kluwer Academic Publishers, Dordrecht, **2002**; b) M. N. Chaur, F. Melin, A. L. Ortiz, L. Echegoyen, *Angew. Chem.* **2009**, *121*, 7650–7675; *Angew. Chem. Int. Ed.* **2009**, *48*, 7514–7538; c) L. Dunsch, S. Yang, *Small* **2007**, *3*, 1298–1320; d) C. R. Wang, T. Kai, T. Tomiyama, T. Yoshida, Y. Kobayashi, E. Nishibori, M. Takata, M. Sakata, H. Shinohara, *Nature* **2000**, *408*, 426–427.

[2] J. R. Heath, S. C. Obrien, Q. Zhang, Y. Liu, R. F. Curl, H. W. Kroto, F. K. Tittel, R. E. Smalley, *J. Am. Chem. Soc.* **1985**, *107*, 7779–7780.

[3] S. Stevenson, G. Rice, T. Glass, K. Harich, F. Cromer, M. R. Jordan, J. Craft, E. Hadju, R. Bible, M. M. Olmstead, K. Maitra, A. J. Fisher, A. L. Balch, H. C. Dorn, *Nature* **1999**, *401*, 55–57.

[4] a) J. M. Campanera, C. Bo, J. M. Poblet, *Angew. Chem.* **2005**, *117*, 7396–7399; *Angew. Chem. Int. Ed.* **2005**, *44*, 7230–7233; b) R. Valencia, A. Rodríguez-Fortea, J. M. Poblet, *Chem. Commun.* **2007**, 4161–4163; c) A. Rodríguez-Fortea, A. L. Balch, J. M. Poblet, *Chem. Soc. Rev.* **2011**, *40*, 3551–3563.

[5] A. A. Popov, L. Dunsch, *J. Am. Chem. Soc.* **2007**, *129*, 11835–11849.

[6] A. Rodríguez-Fortea, N. Alegret, A. L. Balch, J. M. Poblet, *Nature Chem.* **2010**, *2*, 955–961.

[7] P. P. Fatouros, F. D. Corwin, Z. J. Chen, W. C. Broaddus, J. L. Tatum, B. Kettenmann, Z. Ge, H. W. Gibson, J. L. Russ, A. P. Leonard, J. C. Duchamp, H. C. Dorn, *Radiology* **2006**, *240*, 756–764.

[8] E. B. Iezzi, J. C. Duchamp, K. Harich, T. E. Glass, H. M. Lee, M. M. Olmstead, A. L. Balch, H. C. Dorn, *J. Am. Chem. Soc.* **2002**, *124*, 524–525.

[9] J. M. Campanera, C. Bo, . M. Poblet, *J. Org. Chem.* **2006**, *71*, 46–54.

[10] C. M. Cardona, B. Elliott, L. Echegoyen, *J. Am. Chem. Soc.* **2006**, *128*, 6480–6485.

[11] T. Cai, C. Slebodnick, L. Xu, K. Harich, T. E. Glass, C. Chancellor, J. C. Fettinger, M. M. Olmstead, A. L. Balch, H. W. Gibson, H. C. Dorn, *J. Am. Chem. Soc.* **2006**, *128*, 6486–6492.

[12] O. Lukoyanova, C. M. Cardona, J. Rivera, L. Z. Lugo-Morales, C. J. Chancellor, M. M. Olmstead, A. Rodríguez-Fortea, J. M. Poblet, A. L. Balch, L. Echegoyen, *J. Am. Chem. Soc.* **2007**, *129*, 10423–10430.

[13] A. Rodríguez-Fortea, J. M. Campanera, C. M. Cardona, L. Echegoyen, J. M. Poblet, *Angew. Chem.* **2006**, *118*, 8356–8360; *Angew. Chem. Int. Ed.* **2006**, *45*, 8176–8180.

[14] T. Cai, L. S. Xu, M. R. Anderson, Z. X. Ge, T. M. Zuo, X. L. Wang, M. M. Olmstead, A. L. Balch, H. W. Gibson, H. C. Dorn, *J. Am. Chem. Soc.* **2006**, *128*, 8581–8589.

[15] S. Stevenson, M. A. Mackey, C. E. Coumbe, J. P. Phillips, B. Elliott, L. Echegoyen, *J. Am. Chem. Soc.* **2007**, *129*, 6072–6073.

[16] T. Cai, L. Xu, H. W. Gibson, H. C. Dorn, C. J. Chancellor, M. M. Olmstead, A. L. Balch, *J. Am. Chem. Soc.* **2007**, *129*, 10795–10800.

[17] a) T. Cai, L. Xu, C. Shu, H. A. Champion, J. E. Reid, C. Anklin, M. R. Anderson, H. W. Gibson, H. C. Dorn, *J. Am. Chem. Soc.* **2008**, *130*, 2136–2137; b) T. Cai, L. S. Xu, C. Y. Shu, J. E. Reid, H. W. Gibson, H. C. Dorn, *J. Phys. Chem. C* **2008**, *112*, 19203–19208.

[18] S. Osuna, M. Swart, J. M. Campanera, J. M. Poblet, M. Solà, *J. Am. Chem. Soc.* **2008**, *130*, 6206–6214.

[19] S. Osuna, M. Swart, M. Solà, *J. Am. Chem. Soc.* **2009**, *131*, 129–139.

[20] M. Garcia-Borràs, S. Osuna, J. M. Luis, M. Swart, M. Solà, *Chem. Eur. J.* **2012**; DOI: 10.1002/chem.201103701.

[21] N. Alegret, M. N. Chaur, E. Santos, A. Rodríguez-Fortea, L. Echegoyen, J. M. Poblet, *J. Org. Chem.* **2010**, *75*, 8299–8302.

[22] S. Osuna, M. Swart, M. Solà, *Phys. Chem. Chem. Phys.* **2011**, *13*, 3585–3603.

[23] a) E. J. Baerends, J. Autschbach, A. Bérces, F. M. Bickelhaupt, C. Bo, P. L. de Boeij, P. M. Boerrigter, L. Cavallo, D. P. Chong, L. Deng, R. M. Dickson, D. E. Ellis, L. Fan, T. H. Fischer, C. Fonseca Guerra, S. J. A. van Gisbergen, J. A. Groeneveld, O. V. Gritsenko, M. Grüning, F. E. Harris, P. van den Hoek, C. R. Jacob, H. Jacobsen, L. Jensen, G. van Kessel, et al. *ADF 2010.1*, *SCM*, Amsterdam **2010**; b) G. te Velde, F. M. Bickelhaupt, E. J. Baerends, C. Fonseca Guerra, S. J. A. van Gisbergen, J. G. Snijders, T. Ziegler, *J. Comput. Chem.* **2001**, *22*, 931–967.

[24] M. Swart, J. G. Snijders, *Theor. Chem. Acc.* **2003**, *110*, 34–41.

[25] S. H. Vosko, L. Wilk, M. Nusair, *Can. J. Phys.* **1980**, *58*, 1200–1211.

[26] A. D. Becke, *Phys. Rev. A* **1988**, *38*, 3098–3100.

[27] J. P. Perdew, *Phys. Rev. B* **1986**, *33*, 8800–8802.

[28] E. van Lenthe, E. J. Baerends, J. G. Snijders, *J. Chem. Phys.* **1993**, *99*, 4597–4610.

[29] a) T. P. M. Goumans, A. W. Ehlers, K. Lammertsma, E.-U. Würthwein, S. Grimme, *Chem. Eur. J.* **2004**, *10*, 6468–6475; b) M. Swart, M. Solà, F. M. Bickelhaupt, *J. Comput. Chem.* **2007**, *28*, 1551–1560.

[30] M. Swart, F. M. Bickelhaupt, *J. Comput. Chem.* **2008**, *29*, 724–734.

[31] M. Swart, F. M. Bickelhaupt, *Int. J. Quant. Chem.* **2006**, *106*, 2536–2544.

[32] S. K. Wolff, *Int. J. Quantum Chem.* **2005**, *104*, 645–659.

[33] a) J. Lu, R. F. Sabirianov, W. N. Mei, Y. Gao, C.-g. Duan, X. Zeng, *J. Phys. Chem. B* **2006**, *110*, 23637–23640; b) J. Wu, F. Hagelberg, *J. Phys. Chem. C* **2008**, *112*, 5770–5777; c) S. F. Yang, A. Popov, M. Kalbac, L. Dunsch, *Chem. Eur. J.* **2008**, *14*, 2084–2092.

[34] T. Yang, X. Zhao, L.-S. Li, J.-J. Zheng, W.-Y. Gao, *ChemPhysChem* **2012**, *13*, 449–452.

[35] a) R. C. Haddon, *J. Phys. Chem. A* **2001**, *105*, 4164–4165; b) R. C. Haddon, S. Y. Chow, *J. Am. Chem. Soc.* **1998**, *120*, 10494–10496.
[36] R. C. Haddon in *QCPE 508/QCMP11044, QCPE Bull., Vol. 8*, **1988**.
[37] a) J. C. Duchamp, A. Demortier, K. R. Fletcher, D. Dorn, E. B. Iezzi, T. Glass, H. C. Dorn, *Chem. Phys. Lett.* **2003**, *375*, 655–659; b) S. F. Yang, A. A. Popov, L. Dunsch, *Angew. Chem.* **2008**, *120*, 8318–8322; *Angew. Chem. Int. Ed.* **2008**, *47*, 8196–8200.
[38] a) J. M. Campanera, C. Bo, M. M. Olmstead, A. L. Balch, J. M. Poblet, *J. Phys. Chem. A* **2002**, *106*, 12356–12364; b) A. A. Popov, L. Dunsch, *J. Am. Chem. Soc.* **2008**, *130*, 17726–17742.
[39] a) J. Mestres, M. Duran, M. Solà, *J. Phys. Chem.* **1996**, *100*, 7449–7454; b) M. Solà, J. Mestres, J. Martí, M. Duran, *Chem. Phys. Lett.* **1994**, *231*, 325–330.
[40] a) A. A. Popov, L. Dunsch, *Phys. Chem. Chem. Phys.* **2011**, *13*, 8977–8984; b) N. B. Shustova, A. A. Popov, M. A. Mackey, C. E. Coumbe, J. P. Phillips, S. Stevenson, S. H. Strauss, O. V. Boltalina, *J. Am. Chem. Soc.* **2007**, *129*, 11676–11677; c) T. Wakahara, Y. Iiduka, O. Ikenaga, T. Nakahodo, A. Sakuraba, T. Tsuchiya, Y. Maeda, M. Kako, T. Akasaka, K. Yoza, E. Horn, N. Mizorogi, S. Nagase, *J. Am. Chem. Soc.* **2006**, *128*, 9919–9925.
[41] S. M. Bachrach, P. B. White, *J. Mol. Struct. Theochem* **2007**, *819*, 72–78.
[42] S. Osuna, A. Rodríguez-Fortea, J. M. Poblet, M. Solà, M. Swart, *Chem. Commun.* **2012**, *48*, 2486.
[43] E. B. Iezzi, J. C. Duchamp, K. R. Fletcher, T. E. Glass, H. C. Dorn, *Nano Lett.* **2002**, *2*, 1187–1190.
[44] R. Valencia, A. Rodríguez-Fortea, A. Clotet, C. de Graaf, M. N. Chaur, L. Echegoyen, J. M. Poblet, *Chem. Eur. J.* **2009**, *15*, 10997–11009.
[45] N. N. Greenwood, A. Earnshow, *Chemistry of the Elements*, Pergamon, Oxford, **1984**.
[46] M. Krause, L. Dunsch, *Angew. Chem.* **2005**, *117*, 1581–1584; *Angew. Chem. Int. Ed.* **2005**, *44*, 1557–1560.
[47] S. Osuna, M. Swart, M. Solà, *Chem. Eur. J.* **2009**, *15*, 13111–13123.
[48] N. Chen, L. Z. Fan, K. Tan, Y. Q. Wu, C. Y. Shu, X. Lu, C. R. Wang, *J. Phys. Chem. C* **2007**, *111*, 11823–11828.

Received: March 20, 2012
Published online: June 12, 2012

